Influence of iterative reconstruction and dose levels on metallic artifact reduction: A phantom study within four CT systems

J. Greffier, A. Larbi, J. Frandon, P.A. Daviau, J.P. Beregi, F. Pereira

Influence of iterative reconstruction and dose levels on metallic artifact reduction: a phantom study within four CT systems

Short title: **Metallic artifact reduction**

Authors

J. Greffier*, A. Larbi, J. Frandon, P.A. Daviau, J.P Beregi, F. Pereira

All authors: Service d'Imagerie Médicale, CHU Nimes, Univ Montpellier, Medical Imaging Group Nimes, EA 2415,Nimes, France

***Corresponding author**: joel.greffier@chu-nimes.fr

Abstract

Purpose: To compare metallic artifact reduction (MAR) algorithms proposed by four vendors according to the delivered dose and iterative level using a phantom study.

Methods: Four CT systems (Revolution GSI®, Ingenuity Elite®, Somatom Edge®, and Aquilion Prime®) equipped with MAR algorithms (Smart MAR®, O-MAR®, iMAR®, and SEMAR®) were compared. Acquisitions were performed with CIRS Phantom technology containing a titanium rod core insert using 120 kV and two dose levels (3 and 7mGy). Images were reconstructed with and without MAR algorithms using standard "soft tissue" kernel for filtered back projection (FBP) and intermediary iterative level. Artifact propagation was assessed by counting the number of pixels containing an HU outside a defined threshold interval (> 100HU and < -80 HU). Artifact correction was evaluated by computing the differences between images with and without MAR.

Results: Accuracy of N_{CT} values increased significantly using MAR algorithms, IR, and high dose levels (P<0.001). Image noise reduced -31±15 (SD) % (range: -50% ;-14%) with Smart-MAR®, -28 ± 3 (SD) % (range -31%; -25%) with O-MAR®, -32 ± 7 (SD) % (range: -40%; -24%) with $iMAR_{CN}$®, -52 ± 8 (SD) % (range: -60%; -42%) with $iMAR_{TH}$® and -29 ± 6 (SD) % (range: -37%; -23%) with SEMAR®. The number of pixels outside the threshold interval was also reduced using MAR algorithms. Each MAR algorithm corrected in distinct patterns, with satisfactory artifact correction for all MAR algorithms.

Conclusion: This study demonstrates that artifact correction using MAR algorithms differs according to the main manufacturers, although corrections are satisfactory for all systems. Corrections also improved by using IR and increasing the dose level.

Keywords: Metallic artifact reduction (MAR); Computed tomography (CT); Image quality; Iterative reconstruction.

Abbreviations

CT: Computed tomography

FBP: Filtered back projection

iMAR®: iterative metal artifact reduction

IR: Iterative reconstruction

MAR: Metallic artifact reduction

O-MAR®: Metal artifact reduction for orthopedic implants

ROI: Region of iInterest

SEMAR®: Single energy metal artifact reduction

Smart-MAR®: Smart metallic artifact reduction

Introduction

Computed tomography (CT) image quality is degraded in patients with metallic material because of disruptions known as metallic artifacts [1]. These artifacts hinder or even prevent radiologists from evaluating the interface between metallic materials and adjacent tissues. Metallic artifacts result when structures induce profound nonlinearity between measured attenuation projections and attenuation line integrals, leading to beam hardening and photon starvation [2-4]. When a photon beam interacts with metal, low-energy photons are more attenuated than high-energy photons. By contrast, high attenuation leads to insufficient photon quantities reaching the detector). These quantum phenomena distort calculations during the image reconstruction process, resulting in higher image-noise and the presence of dark streaks around the metallic device.

Several simple techniques have been used to reduce metallic artifacts, such as increasing kV or mAs, using softer reconstruction kernel, using iterative reconstructions (IR), using thinner slices, and adapting windowing [1, 5, 6]. However, these techniques have a limited impact on artifact reduction and may require an increased delivered dose or a reduction of spatial resolution. Another strategy to reduce metallic artifact consists of using extrapolated mono-energetic images obtained with dual-energy CT [2, 7-9]. However, dual energy CT-scanners are not widespread, datasets are usually acquired prospectively, and post-processing is time-consuming. Recently, metal artifact reduction (MAR) algorithms have been proposed [2-4, 10-14]. MAR aims to reduce artifacts caused by beam hardening and photon starvation. Algorithms are split in two groups: sinogram completion methods such as projection-based MAR, and model-based iterative algorithms [3, 15]. In both, metal objects are segmented in raw-data space (sinogram) and replaced by approximated or interpolated data [14, 16-19]. MAR algorithms can be used with single or dual energy CT systems.

Many studies have demonstrated the clinical contribution of these algorithms on artifact reduction [2-4, 10-14]. However, the majority of these studies were performed using a

single MAR algorithm. Other studies compared different MAR algorithms for the same dose level and type of reconstruction (filtered back projection [FBP] or IR). Therefore, an important emerging question is how MAR algorithms influence metallic artifact corrections with respect to dose reduction and use of IR algorithms.

The purpose of this study was to compare MAR algorithms proposed by four vendors according to the delivered dose and iterative level using a phantom study.

Materials and methods

CT examinations

Datasets were acquired using four distinct CT systems including Revolution GSI® (GE Healthcare), Ingenuity Elite® (Philips Medical Systems), Somatom EDGE® (Siemens Healthineers) and Aquilion Prime® (Canon Medical Systems). The CT units were equipped with the following MAR algorithms: Smart-MAR® (GE Healthcare), SEMAR® (Canon Medical Systems), iMAR® (Siemens Healthineers) and O-MAR® (Philips Medical Systems). The basic principle of the first two MAR algorithms relies on projection-based MAR whereas the last two rely on model-based iterative algorithms.

Phantom features

The model 062M electron density phantom (CIRS) was used. This phantom has two nested disks (head and abdomen) made of Plastic Water® in which 17 different inserts with 30-mm diameter can be used to simulate human tissue or medical objects. The titanium rod core insert was employed to assess MAR algorithms. This cylindrical insert has a diameter of 6.35mm and a high electron density (12.475×10^{23} electrons/cm^3). These characteristics are similar to a coil employed for cerebral or abdominal embolization. Positions of 17 inserts are shown in Figure 1a. Titanium insert was placed in the lateral part of the abdomen disk (Figure 1b), configuration employed for all acquisitions.

Parameters of acquisition and reconstruction

Acquisitions were performed with rotation time of 0.5s/rot and tube current modulation was disabled. Tube voltage was 120kV and tube current (mAs) was adjusted to obtain a volume computed tomography dose index (CTDIvol) determined for a 32 cm-diameter reference phantom of 3.0 and 7.0mGy, corresponding to the delivered dose in our institution for

thoracic and abdominal-pelvic acquisitions, respectively. Acquisitions were performed on helical mode with a pitch factor close to 1, which corresponds to the intermediary pitch factor between thoracic and abdominal-pelvic acquisitions.

Raw data were reconstructed using "soft tissue" kernel, with FBP and intermediate iterative level of IR algorithm available on each system and used in clinical practice (Asir-V® for GE Healthcare, iDose^{4}® for Philips Medical Systems, ADMIRE® for Siemens Healthineers and AIDR 3D® for Canon Medical Systems). Hybrid or statistical IR algorithms were used in all systems, except for Somatom Edge®. ADMIRE® corresponds to a partial model-based iterative reconstruction.

Images were reconstructed with and without MAR algorithms, with a field-of-view of 350mm and slice thickness close to 1mm. For Somatom Edge®, seven types of artifact correction were available with iMAR® algorithms. Neuro coils (iMAR$_{NE}$®) and thoracic coils (iMAR$_{TH}$®) were evaluated in this study. These two types of algorithms are usually used to correct metal artifacts generated by cerebral, thoracic and abdominal coils. Acquisition and reconstruction parameters are shown in Table 1. The total number of reconstructed data sets evaluated was 36, corresponding to eight for each system assessed, except for Somatom Edge® (12).

Raw images were stored in 12 bits except for Aquilion Prime®, which had data stored in 16 bits. The scale of HU values can be represented with 4096 gray levels for 12 bits and 65536 gray levels for 16 bits.

CT-number and image-noise

Image-quality evaluations were performed using in-house MATLAB® routines. Two square regions-of-interest (ROI) were centered in the titanium rod core insert (Figure 1c): a ROI of 11x11 pixels surrounds the insert (ROI_{Insert}) and a ROI of 45x45 pixels includes the Plastic Water® and the titanium insert (ROI_{Tot}). A third ROI ($ROI_{Tot-Insert}$) was defined by using all pixels contained in ROI_{Tot} except the pixels inside the ROI_{Insert}. This $ROI_{Tot-Insert}$ was composed only with Plastic Water® ($N_{CT} \approx 10HU$). Average and standard deviation of the pixel values were computed in $ROI_{Tot-Insert}$. The former corresponds to the mean of CT-number (N_{CT}) and the latter to the image-noise (standard deviation of N_{CT} value).

Accuracy of N_{CT} was assessed by means of pixel value distribution in the $ROI_{Tot\text{-}Insert}$. Median, 1st and 3rd quartiles were computed. This assessment indicates the variability of N_{CT} values within $ROI_{Tot\text{-}Insert}$.

Horizontal and vertical profiles

Horizontal and vertical profiles were defined as the pixel values extracted from horizontal and vertical lines passing through the center of the insert. Full-width at half-maximum (FWHM) was used to estimate insert diameters. Profile baseline values were defined according to the mean value of N_{CT} in the $ROI_{Tot\text{-}insert}$ that correspond to the mean HU values out of the insert depicted in the bottom line of the profile. Profile maximum values were obtained from the mean of N_{CT} within the ROI_{Insert} that correspond to the mean HU values in the insert depicted in the top line of the profile. Differences in percentage between the real and measured diameters were computed.

Artifact propagation

Two assessments were conducted to evaluate artifact dispersion and impact of MAR algorithms. First, two threshold values were employed to catch disturbance of N_{CT} values targeting to HU extreme values. Pixels with values higher than 100HU and lower than -80HU in the ROI_{Tot} were recovered and quantified. Threshold interval was defined using mean and standard deviation of N_{CT} measured in the $ROI_{Tot\text{-}Insert}$ for all CT-scans (10 ± 90 HU). Similar approaches were employed in preceding studies (3, 11). Second, the difference between 'with' and 'without' MAR was computed using $ROI_{Tot.}$ Hot-colors indicate N_{CT} values in the MAR image that are higher than without MAR. Cold-colors were assigned for the opposite.

Statistical analysis

The Kolmogorov-Smirnov (KS) test was used to test data normality. Conover squared-ranks test, a non-parametric test primarily used to identify differences on variability between groups, was used to examine data dispersion (equality of variance). N_{CT} values in $ROI_{Tot\text{-}Insert}$ with and without MAR algorithms for each dose level and reconstruction type were independently compared. The same assessment was employed for 3 mGy versus 7 mGy, for FBP versus IR, and for $iMAR_{NE}$® versus $iMAR_{TH}$®. The Bonferroni test was used correct for multiple comparisons and only *P* values < 0.001 were considered significant.

Results

A test for normality (KS) indicated that the data of this study do not fit normal distribution. Therefore, a non-parametric test (i. e., Conover squared-ranks test) was employed to examine dispersion of N_{CT} values in $ROI_{Tot\text{-}Insert}$.

Mean CT-Number and image-noise

N_{CT} accuracy within $ROI_{Tot\text{-}Insert}$ increased when MAR algorithms were used. Similarly, improved accuracy was found in IR faced to FBP and at 7 mGy compared to 3 mGy. These patterns were found for all CT systems except for Aquilion Prime®, where accuracy reduction was a function of dose delivered (Figure 2).

The median of N_{CT} values was negative for images without iMAR® but positive for images using iMAR® independent of dose level and reconstruction type. In addition, the median of N_{CT} values was higher using $iMAR_{NE}$® than $iMAR_{TH}$®. The median of N_{CT} values was negative for images without SEMAR® but positive using SEMAR® for images reconstructed with FBP, and the opposite was true using IR.

The dispersion of pixel values in $ROI_{Tot\text{-}Insert}$ using MAR algorithms were significantly different (*P-corrected*<0.001) from without using MAR algorithms, independently of dose level and reconstruction type. Additionally, data dispersion had significant differences (*P-corrected* <0.001) for 3 mGy versus 7 mGy and for FBP versus IR, independently of employing MAR algorithms.

Image-noise in $ROI_{Tot\text{-}Insert}$ decreased using MAR algorithms, IR, and high dose (Figure 3). Smart-MAR® algorithm reduced image-noise, and this reduction was greater at 3mGy than 7mGy with IR rather than FBP (-27% for FBP/3mGy, -14% for FBP/7mGy, -50% for IR/3mGy and -35% for IR/7 mGy). O-MAR® algorithm reduced image-noise similarly for dose level and reconstruction type, achieving a mean of -28±3 (SD) % (range: -31%; -25%). SEMAR® algorithm reduced image-noise and this reduction was greater at 7mGy than 3mGy and with IR rather than FBP (-23% for FBP/3mGy, -29% for FBP/7mGy, -28% for IR/3mGy and -37% for IR/7 mGy). For Somatom Edge®, a similar pattern was found and image noise reduction was more evident with $iMAR_{TH}$® (-42% for FBP/3mGy, -49% for FBP/7mGy, -57% for IR/3mGy and -60% for IR/7 mGy) than $iMAR_{NE}$® (-24% for FBP/3mGy, -31% for FBP/7mGy, -34% for IR/3mGy and -40% for IR/7 mGy).

Horizontal and vertical profiles

For images not using MAR algorithms, measured diameters were higher than actual insert diameters in Revolution GSI®, Ingenuity Elite® and Somatom Edge®, but lower in Aquilion Prime® (Table 2). Vertical diameter was slightly higher (from 4 to 8%) than horizontal diameter for Revolution GSI®, Ingenuity Elite® and Somatom Edge® independently of MAR algorithm usage. Additionally, for the Revolution GSI®, both diameters were reduced using Smart-MAR® (-15% for horizontal and -18% for vertical diameter) compared to no MAR, resulting in a smaller insert image than real one. For other CT systems, diameter variations were less noticeable using MAR algorithms ($\leq \pm 2\%$).

Artifact propagation

The number of pixels below -80HU or above 100HU decreased using MAR algorithms except for $iMAR_{TH}$®, in which the number of pixels was similar with no MAR (Figure 4). For the Somatom Edge® with iMAR®, reduction of pixel numbers below -80HU was greater than pixels above 100HU. Moreover, the number of pixels within the interval decreased from IR to FBP and from 7mGy versus 3mGy, with the exception of Aquilion Prime®, where the number of pixels was higher at 7mGy than at 3mGy.

Discussion

Metallic artifacts are a major concern for radiologists because they complicate or even prevent radiological evaluation. Image evaluation of the interface between the metallic materials and adjacent tissues is particularly problematic [1]. MAR algorithms have emerged as important tools to reduce metallic artifacts without increasing delivered dose or decreasing spatial resolution [1, 5, 6]. Preceding studies have assessed the impact of these algorithms on phantoms and on clinical practice [2-4, 10-14]. However, few studies have compared distinct MAR algorithms according to dose levels and using FBP and IR. Additionally, radiological studies evaluating whether and how artifacts are created from coil devices are lacking. This experimental study aimed to objectively evaluate image-quality of MAR algorithms in GE Healthcare®, Philips Medical systems®, Siemens Healthineers® and Canon Medical Systems® as a function of dose level and reconstruction type.

Although accuracy of N_{CT} values depends on material density, MAR algorithms improve such metric and reduce image-noise in $ROI_{Tot\text{-}Insert}$. These findings are significantly more pronounced for IR versus FBP and when dose increases in all but Aquilion Prime®.

Similar results were published regarding N_{CT} accuracy and image-noise reduction [2, 4, 11, 14]. However, these studies were carried out with orthopedic or dental implants of different size and/or composition.

Insert deformation was evaluated as a function of reconstruction type, dose levels and MAR algorithms. For Revolution GSI®, Somatom Edge® and Aquilion Prime®, inserts were distorted with and without MAR algorithms. Moreover, vertical diameter was higher than the horizontal diameter. MAR algorithms had no impact on measured insert diameters, except in the instance of GE, where Smart-MAR® reduced insert diameter in both axes. Similar results were found by Huang *et al.* [11]. Furthermore, insert was not distorted using IR or when dose decreases.

Artifact propagation and prevalence of bright/dark streaks were assessed. MAR algorithms reduced pixel count outside of the -80HU to 100HU threshold range, except for iMAR®$_{TH}$ with N_{CT} < -80HU. Bolstad *et al.* [3] presented similar results for titanium inserts thresholded at 500HU using Smart-MAR®, iMAR® (in hip implant) and SEMAR®.

The visual impact of MAR algorithms on metal artifact correction and image quality is shown in Figure 5 and Figure 6. Smart-MAR® and SEMAR® typically reduce dark streaks thereby increasing pixel values around the insert, although some pixel values were reduced forming a “black circle”. The effect of having a “black circle” around the insert improves transition between solid water and metal. For SEMAR®, pixel values increased around the insert whereas those in periphery reduced. For Ingenuity Elite® system, increasing and reducing pixel values had equal rates.

Decreased values around the insert were also observed. With iMAR®, the pixel values on the periphery of the insert reduced. Corrections were more pronounced with iMAR$_{TH}$® than iMAR$_{NE}$®, but the image-quality appears higher with iMAR$_{NE}$®. Berger *et al.* found that iMAR$_{NE}$® presented better results than iMAR$_{TH}$® in correcting artifacts due to metal residues [20].

This study has some limitations. First, raw-data were reconstructed using a single kernel and one iterative level. Second, it was carried out on a 6.35mm titanium insert that could have similar features of brain or abdominal coil. This study hypothesized that metallic artifact produced by this insert would be comparable to those produced by these coils. However, this hypothesis needs to be validated in a clinical study. Third, only phantom was

employed, thus the same study should be performed on patients. Finally, spatial resolution was not assessed.

In conclusion, our results suggest that MAR algorithms correct artifacts generated by an insert similar to cerebral or abdominal coils. Correction improves accuracy of N_{CT} and bright/dark streaks, but also modifies the insert. Moreover, correction patterns differ across manufacturers. In addition, the efficiency of MAR algorithms improves using IR and decreases when the dose decreases.

Conflict of interests

The authors have no conflicts of interest to disclose regarding this article.

REFERENCES

[1] Barrett JF, Keat N. Artifacts in CT: recognition and avoidance. Radiographics 2004;24:1679-91.

[2] Andersson KM, Nowik P, Persliden J, Thunberg P, Norrman E. Metal artefact reduction in CT imaging of hip prostheses-an evaluation of commercial techniques provided by four vendors. Br J Radiol 2015;88:20140473.

[3] Bolstad K, Flatabo S, Aadnevik D, Dalehaug I, Vetti N. Metal artifact reduction in CT, a phantom study: subjective and objective evaluation of four commercial metal artifact reduction algorithms when used on three different orthopedic metal implants. Acta Radiol 2018;59:1110-8.

[4] Morsbach F, Bickelhaupt S, Wanner GA, Krauss A, Schmidt B, Alkadhi H. Reduction of metal artifacts from hip prostheses on CT images of the pelvis: value of iterative reconstructions. Radiology 2013;268:237-44.

[5] Lee MJ, Kim S, Lee SA, Song HT, Huh YM, Kim DH, et al. Overcoming artifacts from metallic orthopedic implants at high-field-strength MR imaging and multi-detector CT. Radiographics 2007;27:791-803.

[6] Nakae Y, Sakamoto K, Minamoto T, Kamakura T, Ogata Y, Matsumoto M, et al. Clinical evaluation of a newly developed method for avoiding artifacts caused by dental fillings on X-ray CT. Radiol Phys Technol 2008;1:115-22.

[7] Bamberg F, Dierks A, Nikolaou K, Reiser MF, Becker CR, Johnson TR. Metal artifact reduction by dual energy computed tomography using monoenergetic extrapolation. Eur Radiol 2011;21:1424-9.

[8] Lewis M, Reid K, Toms AP. Reducing the effects of metal artefact using high keV monoenergetic reconstruction of dual energy CT (DECT) in hip replacements. Skeletal Radiol 2013;42:275-82.

[9] Meinel FG, Bischoff B, Zhang Q, Bamberg F, Reiser MF, Johnson TR. Metal artifact reduction by dual-energy computed tomography using energetic extrapolation: a systematically optimized protocol. Invest Radiol 2012;47:406-14.

[10] Hu Y, Pan S, Zhao X, Guo W, He M, Guo Q. Value and clinical application of Orthopedic Metal artifact reduction algorithm in CT scans after orthopedic metal implantation. Korean J Radiol 2017;18:526-35.

[11] Huang JY, Kerns JR, Nute JL, Liu X, Blater PA, Stingo FC, et al. An evaluation of three commercially available metal artifact reduction methods for CT imaging. Phys Med Biol 2015;60:1047-67.

[12] Jeong S, Kim SH, Hwang EJ, Shin CI, Han JK, Choi BI. Usefulness of a metal artifact reduction algorithm for orthopedic implants in abdominal CT: phantom and clinical study results. AJR Am J Roentgenol 2015;204:307-17.

[13] Kidoh M, Nakaura T, Nakamura S, Tokuyasu S, Osakabe H, Harada K, et al. Reduction of dental metallic artefacts in CT: value of a newly developed algorithm for metal artefact reduction (O-MAR). Clin Radiol 2014;69:e11-6.

[14] Yasaka K, Maeda E, Hanaoka S, Katsura M, Sato J, Ohtomo K. Single-energy metal artifact reduction for helical computed tomography of the pelvis in patients with metal hip prostheses. Jpn J Radiol 2016;34:625-32.

[15] Giantsoudi D, De Man B, Verburg J, Trofimov A, Jin Y, Wang G, et al. Metal artifacts in computed tomography for radiation therapy planning: dosimetric effects and impact of metal artifact reduction. Phys Med Biol 2017;62:R49-80.

[16] Hauswald H, Bär E, Reducing mater artifacts in a patient with dental fillings. SOMATOM Session. 2014; Radiation Therapy Supplement.

[17] GE Healthcare. Smart metal artifact reduction (MAR). wwwgehealthcarecom/MAR, 2013.

[18] Philips Healthcare - Philips CT Clinical Science: metal artifact reduction for orthopedic implant (O-MAR), White Paper, 2017.

[19] Gondim Teixeira PA, Meyer JB, Baumann C, Raymond A, Sirveaux F, Coudane H, et al. Total hip prosthesis CT with single-energy projection-based metallic artifact reduction: impact on the visualization of specific periprosthetic soft tissue structures. Skeletal Radiol 2014; 43:1237-46.

[20] Berger F, Niemann T, Kubik-Huch RA, Richter H, Thali MJ, Gascho D. Retained bullets in the head on computed tomography - Get the most out of iterative metal artifact reduction. Eur J Radiol 2018;103:124-30.

Figure legends

Figure 1: a. Positions of the 17 inserts in the two nested disks; b. CT image of the phantom with its 17 inserts; c. ROIs used in this study. Red corresponds to the ROITot of 45×45 pixels; yellow to the ROIInsert of 11×11 pixels. ROITot-insert corresponds to the pixels within the red square excluding the yellow.

Figure 2. Accuracy of N_{CT} values was computed in $ROI_{Tot\text{-}Insert}$ for images with/without MAR algorithms of four manufacturers as function of the dose and the reconstruction type. Bars are defined by means of the lower box end (1st quartile: Q1, the margin of the lower and upper box (median and the upper box line (3rd quartile: Q3. The expected N_{CT} value of Plastic Water is approximatively 10HU.

Figure 3. Image-noise values computed in $ROI_{Tot\text{-}Insert}$ for images with/without MAR algorithms of four manufacturers as function of the dose and the reconstruction type.

Figure 4. Number of pixels with N_{CT} values inferior to -80HU or superior to 100HU for images with/without MAR algorithms of four manufacturers as function of the dose and the reconstruction type.

Figure 5. Image-quality in ROI_{Tot} of 45×45 pixels centered on the titanium insert for images with/without MAR algorithms of four manufacturers as function of the dose and the reconstruction type. The window and level were fixed to 350 HU and 50 HU, respectively. This figure illustrates artifact propagation before correction and respective artifact reduction. Dark/bright streaks around the metal device were found in images without MAR algorithms. Bright streaks were globally corrected using MAR algorithms. The dark circle surrounding the insert was found using Smart-MAR®. A blurred zone was created using $iMAR_{NE}$® and dark streaks appeared on either side of the insert using $iMAR_{TH}$®. For Aquilion Prime® system, images were smoothed using IR.

Figure 6. Difference between images in ROI_{Tot} of 45×45 pixels with and without MAR algorithms of four manufacturers as function of the dose and the reconstruction type. Hot colors were assigned to all pixels having N_{CT} values in MAR image higher than image without MAR. Cold colors were assigned for the reverse situation. This figure illustrates differences between images with and without MAR. Red streaks, corresponding to pixels with higher values in MAR images than without MAR images, were found for all manufacturers. Blue streaks, corresponding to pixels with lower values in MAR images than without MAR images, were observed in images using O-MAR® and $iMAR_{TH}$®. Lastly, pixel values on the insert borders decreased using MAR algorithms. Both red and blue colors had greater intensity with $iMAR_{TH}$® than $iMAR_{NE}$ ®.

Table 1. Acquisition and reconstruction parameters used on each CT unit.

Table 2. Differences in percentage between the unique diameter of the titanium rod core insert (6.35 mm) and the horizontal and vertical diameters obtained for dose levels and reconstruction types.

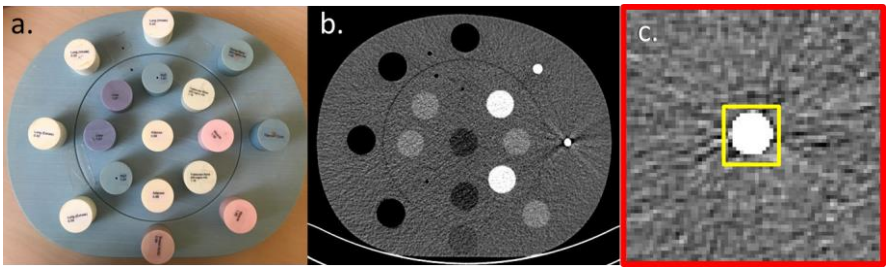
a.
b.
c.

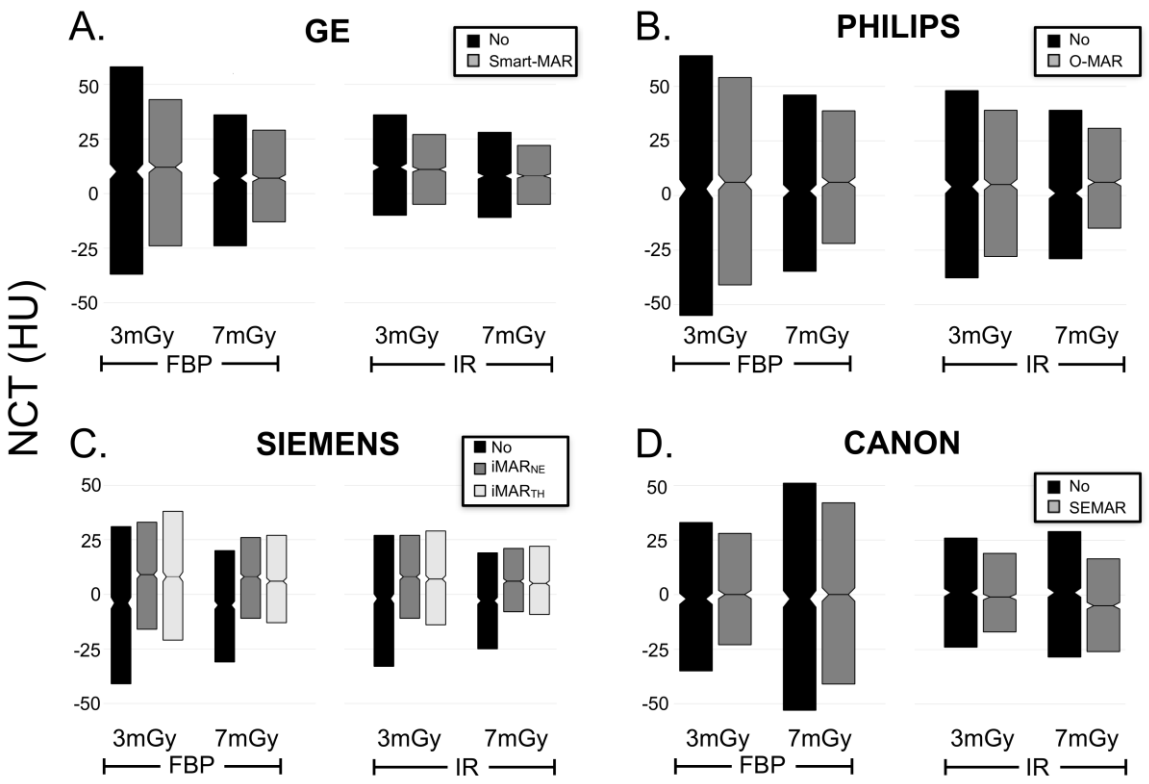
A.
GE
No
Smart-MAR
B.
PHILIPS
No
O-MAR
C.
SIEMENS
No
iMAR$_{NE}$
iMAR$_{TH}$
D.
CANON
No
SEMAR
NCT (HU)
50
25
0
-25
-50
3mGy
7mGy
FBP
IR

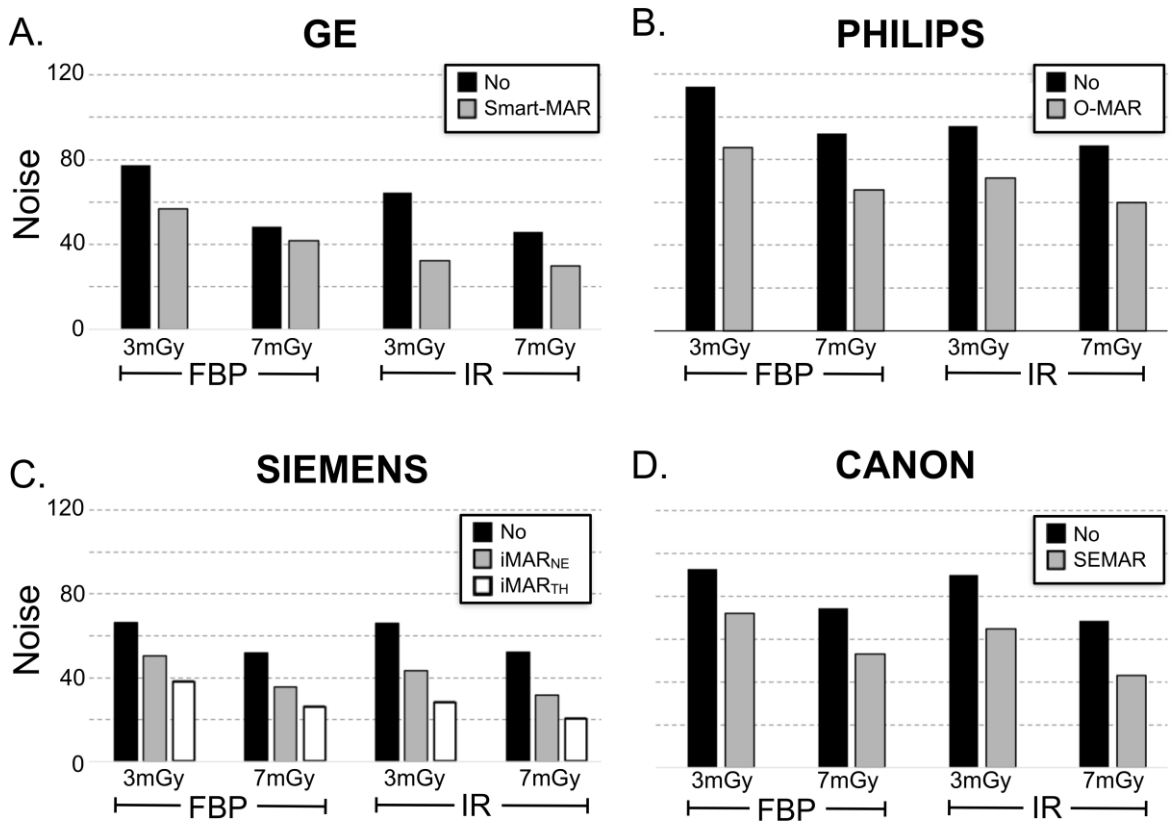
A.
GE
120
80
40
0
Noise
No
Smart-MAR
3mGy
7mGy
3mGy
7mGy
FBP
IR
B.
PHILIPS
No
O-MAR
3mGy
7mGy
3mGy
7mGy
FBP
IR
C.
SIEMENS
120
80
40
0
Noise
No
iMAR$_{NE}$
iMAR$_{TH}$
3mGy
7mGy
3mGy
7mGy
FBP
IR
D.
CANON
No
SEMAR
3mGy
7mGy
3mGy
7mGy
FBP
IR

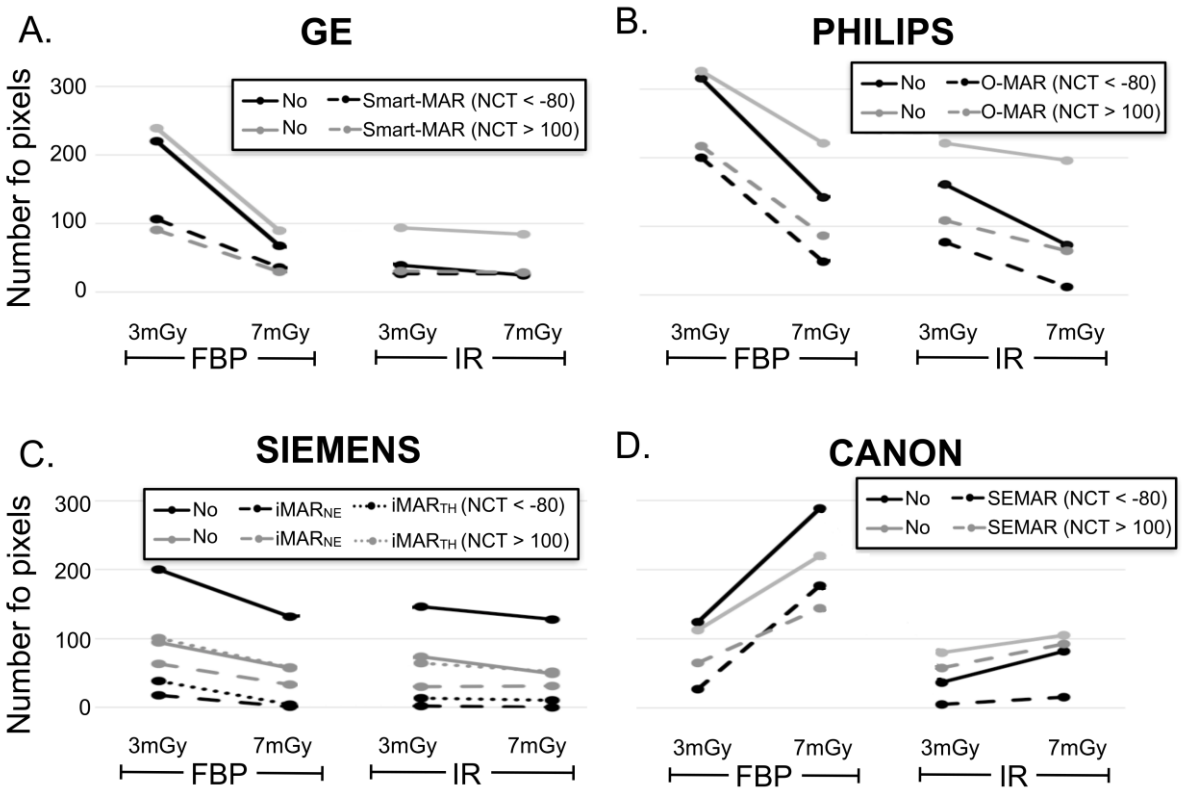
A.
GE
Number fo pixels
300
200
100
0
No
Smart-MAR (NCT < -80)
No
Smart-MAR (NCT > 100)
3mGy
7mGy
3mGy
7mGy
FBP
IR
B.
PHILIPS
No
O-MAR (NCT < -80)
No
O-MAR (NCT > 100)
3mGy
7mGy
3mGy
7mGy
FBP
IR
C.
SIEMENS
Number fo pixels
300
200
100
0
No
iMAR$_{NE}$
iMAR$_{TH}$ (NCT < -80)
No
iMAR$_{NE}$
iMAR$_{TH}$ (NCT > 100)
3mGy
7mGy
3mGy
7mGy
FBP
IR
D.
CANON
No
SEMAR (NCT < -80)
No
SEMAR (NCT > 100)
3mGy
7mGy
3mGy
7mGy
FBP
IR

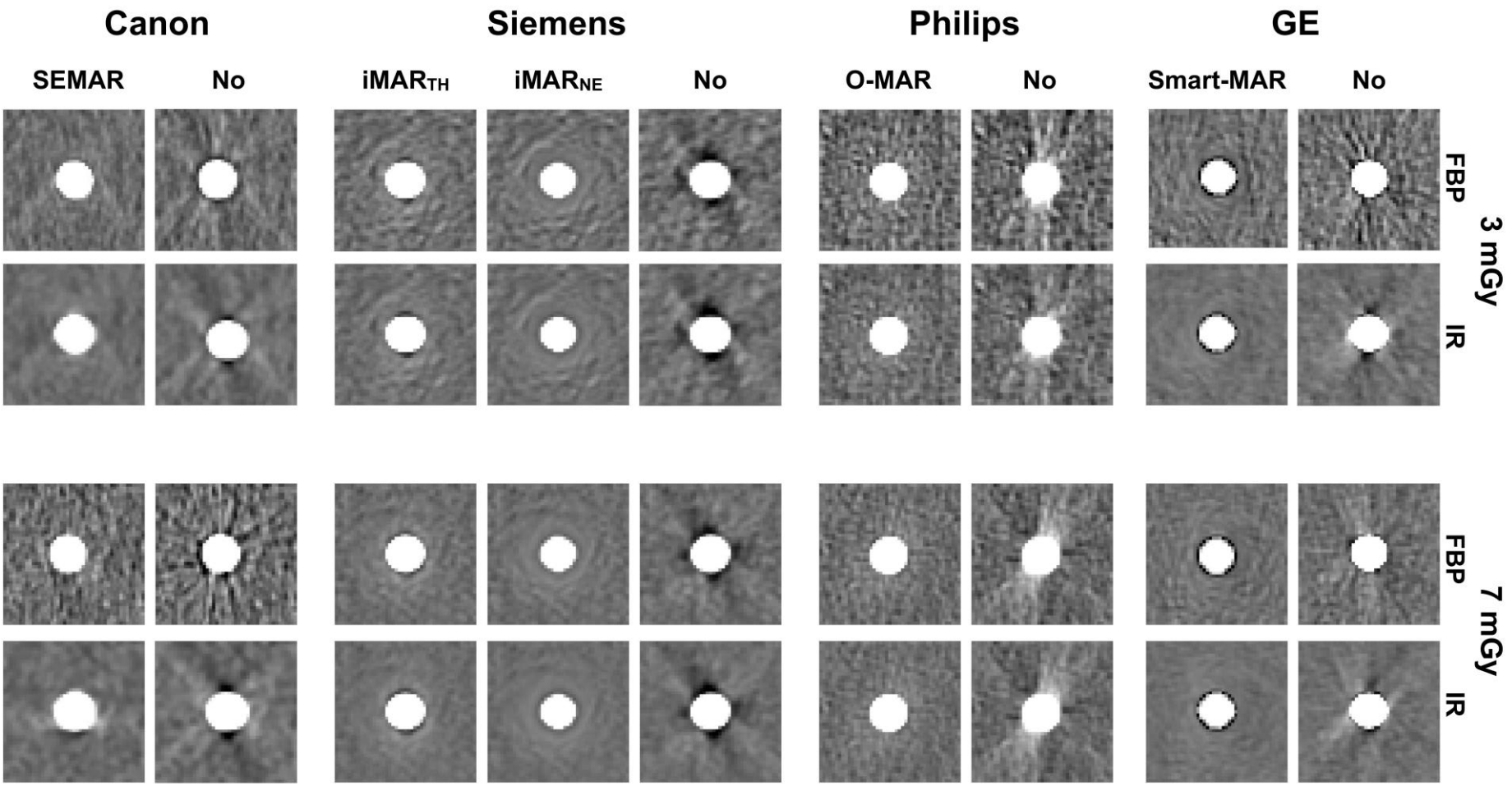
Canon
Siemens
Philips
GE
SEMAR
No
iMARTH
iMARNE
No
O-MAR
No
Smart-MAR
No
FBP
IR
3 mGy
FBP
IR
7 mGy

3 mGy
7 mGy
FBP
IR
FBP
IR
GE
Smart-MAR - No
Philips
O-MAR - No
Siemens
iMAR$_{NE}$ - No
iMAR$_{TH}$ - No
Canon
SEMAR - No

Manufacturer	GE Healthcare	Philips Medical Systems	Siemens Healthineers	Canon Medical Systems
Model	Revolution® GSI	Ingenuity® Elite	Definition® EDGE	Aquilion® Prime
Collimation (mm)	64 × 0.625	64 × 0.625	64 × 0.6	80 × 0.5
mA value adjusted for 3mGy	70	91	90	50
mA value adjusted for 7mGy	160	211	208	120
Pitch	0.984	0.985	1	0.813
Iterative algorithm and level	ASIR-V 50%	iDose^4 Level 3	ADMIRE Level 3	AIDR Standard
Soft kernel	Standard	B	B/I30f	FC17
Thickness/overlapped (mm/mm)	1.25/1.25	1/1	1/1	1/1
MAR	Smart Metal Reduction Artifact (Smart-MAR)	Metal Artifact Reduction for Orthopedic Implants (O-MAR)	iterative Metal Artifact Reduction (iMAR)*	Single Energy Metal Artifact Reduction (SEMAR)
Bits stored	12	12	12	16

* Seven types of artifact corrections are available with iMAR® algorithm. Neuro coils ($iMAR_{NE}$®) and thoracic coils ($iMAR_{TH}$®) were evaluated in this study.

		Diameter variation (%)	
		Horizontal	Vertical
GE Healthcare	No	8 ± 0 [7.6; 8.5]	16 ± 2 [13.6; 18.4]
	Smart-MAR	-7 ± 2 [-8.4; -3.9]	-2 ± 1 [-3.5; -0.5]
Philips Medical Systems	No	13 ± 0 [12.5; 13.2]	13 ± 1 [12.9; 14.3]
	O-MAR	11 ± 0 [10.9; 11.2]	12 ± 0 [11.7; 12.4]
Siemens Healthineers	No	11 ± 1[10.2; 12.4]	16 ± 1 [15.9; 17.2]
	$iMAR_{NE}$	11 ± 1[10.0; 12.2]	15 ± 0 [14.5; 14.7]
	$iMAR_{TH}$	11 ± 1 [10.3; 12.6]	17 ± 1 [16.0; 17.3]
Canon Medical Systems	No	-14 ± 11 [-29.7; -5.9]	-6 ± 6 [-15.3; -2.8]
	SEMAR	-13 ± 5 [-20.1; -8.4]	-8 ± 2 [-12.8; -8.0]

Results are expressed as mean ± standard deviation. Numbers in brackets are ranges.